Applied Catalysis B: Environmental 239 (2018) 513–524

Contents lists available at ScienceDirect

Applied Catalysis B: Environmental

journal homepage: www.elsevier.com/locate/apcatb

Revealing the pathways of catalyst deactivation by coke during the hydrodeoxygenation of raw bio-oil

Tomás Cordero-Lanzac[a], Roberto Palos[a], Idoia Hita[a,b], José M. Arandes[a], José Rodríguez-Mirasol[c], Tomás Cordero[c], Javier Bilbao[a], Pedro Castaño[a,*]

[a] Department of Chemical Engineering, University of the Basque Country (UPV/EHU), PO Box 644-48080, Bilbao, Spain
[b] Chemical Engineering Department, University of Groningen, Nijenborgh 4, 9747 AG, Groningen, The Netherlands
[c] Universidad de Málaga, Department of Chemical Engineering, Andalucia Tech., Campus de Teatinos s/n, 29010, Málaga, Spain

ARTICLE INFO

Keywords:
Hydrodeoxygenation (HDO)
Bio-oil
Metal supported catalyst
Catalyst deactivation
Coke formation
Mechanisms

ABSTRACT

Virtually all processes aiming for fuels and chemicals from biomass entail no less than one step for removing oxygen by hydrodeoxygenation (HDO). The bottleneck of HDO is the formation of deactivating carbonaceous species on the catalyst surface. In this work, we have studied the deactivation pathways of catalysts based on noble metal nanoparticles (Pt-Pd) supported on mildly acid supports during the HDO of raw bio-oil. At conditions of accelerated deactivation, monitoring the evolution with time on stream of hydrocarbon and oxygenated compounds in the reaction medium, the intermediates on the catalyst surface and the nature-location of deactivating species, two parallel deactivation routes have been revealed: the deposition of (i) thermal or pyrolytic lignin from alkylmethoxy phenols, on the catalyst mesopores and favored at low temperature, and; of (ii) aromatic coke from polycyclic aromatic hydrocarbons, starting on the catalyst micropores through condensation reactions and promoted by acidic sites and high temperature. Nevertheless, catalyst deactivation can be controlled within limits at harsh temperature conditions (450 °C) due to the preferential HDO of alkyl(methoxy) phenols into aromatics and the formation-hydrocracking steady state of the aromatic precursors of coke.

1. Introduction

Bio-oil (liquid product of biomass fast pyrolysis) is getting great attention as an alternative source to petroleum for a more sustainable production of fuels and platform chemicals [1]. Nevertheless, oxygen removal through hydrodeoxygenation (HDO) is a required operation in order to stabilize it before its storage [2], and make the most of its great potential as a fuel [3] or as a feedstock in new or conventional refinery units [4–6]. Essentially, all biomass-derived streams for producing fuels and chemicals show similar HDO requirements. The HDO of bio-oil is commonly carried out over Ni, Mo or W supported catalysts [7–13]. However, noble metal-based catalysts (Pt, Pd, Rh or Ru) [14–20], as well as supported bimetallic catalysts [21,22], show higher activity for HDO and allow for using less severe operational conditions. In these works in the literature, the use of both neutral (α-alumina) and acid (activated carbon, γ-alumina, silica-alumina) supports (thus forming metallic or bifunctional catalysts) have been reported for the preparation of the catalysts.

One of the main drawbacks of this reaction is the catalyst deactivation due to the formation of carbonaceous deposits (coke), which also causes operational difficulties [23–28]. This formation of coke is related to the thermal instability and repolymerization of the phenolic components of bio-oil. In this regard, the use of noble metal-based catalysts (especially Pt catalysts) is recommended for attenuating the deactivation since they promote the hydrocracking of coke precursors [24]. Moreover, recent works have shown interesting results of HDO using a two-stage process formed by sequenced mild and deep HDO [29–31]. In both cases, noble metals are commonly used (mainly in the first stage where deactivation is of critical importance and low temperatures are required) and the positive effect of stabilizing the bio-oil in a prior step was demonstrated to favor the production of liquid hydrocarbons in the second one. This configuration has been deeply investigated by the group of Elliott [29–31] attaining hydrocarbon yields of ca. 50 wt%, which evidences its attractiveness. Other authors have proposed modifications in the pyrolysis stage (catalytic pyrolysis [32–34] or hydropyrolysis [35,36], among others) in order to improve the stability of the feedstock and the operability of HDO.

Another significant hurdle is the high content of water in the reaction medium due to its presence in the raw bio-oil (> 50 wt%) [28,37] and its formation during the HDO reaction. In addition to their

* Corresponding author.
E-mail address: pedro.castano@ehu.eus (P. Castaño).

https://doi.org/10.1016/j.apcatb.2018.07.073
Received 27 May 2018; Received in revised form 23 July 2018; Accepted 27 July 2018
Available online 29 July 2018
0926-3373/

low cost of production and sustainable nature, activated carbons (ACs) show a hydrophobic character and high hydrothermal resistance [38,39]. Moreover, the possibility for tailoring their porous texture [39,40] and modifying their surface functional groups [41,42] allows for controlling some catalytic properties such as the dispersion of the metallic particles [43]. Some functionalized ACs present a well-developed mesoporosity that favors the swept of both water and coke precursors outside of the catalyst particle, and therefore their use has been broadly studied as one of the most attractive supports for the HDO of bio-oil [2,12,14–18,44,45]. Nevertheless, the intrisic nature of carbon-based catalysts hinders the characterization of the carbonaceous deposits and their regeneration through combustion. This requires using appropriate techniques for characterizing the coke and favoring its selective combustion, as reported in a previous work, where the possibilities of recovering the properties of the catalyst and the reusability of this kind of catalysts were discussed [46]. In spite of this, the recovery of noble metals is proposed as one of the most attractive strategies in order to manage spent hydroprocessing catalysts [47], either through combustion or gasification of the carbon support [48,49].

Several pathways have been proposed for the HDO of the representative oxygenates of bio-oil: acetone [8,50], acetic acid [44], phenol and alkyl phenols [51–54], guaiacol [45,55–57], cresol [44,57] or anisole [55–57]. These studies also reported the important effect of the feedstock composition and the catalyst properties on coke formation routes and catalyst deactivation [58–60]. Nevertheless, understanding both the HDO and coke formation pathways is complicated when raw bio-oil is fed because of the hundreds of simultaneous reactions and synergies involved in the overall mechanism [44]. This complex condensation and repolymerization reaction network that yields solid deposits can partially be solved for the industrial implementation of HDO by the stabilization of bio-oil [29,32]. However, sequenced treatment of bio-oil hinders for proposing an overall mechanism for catalyst deactivation that considers all the causes of deactivation from bio-oil.

In a previous work, the performance of a Pt-Pd catalyst supported on an activated carbon with acidic sites and highly hydrothermal resistance was studied in the HDO of raw bio-oil [37]. Insights into the presence of different carbonaceous species deposited on the used catalysts were gathered, as well as the role of the reaction conditions in catalyst deactivation. The main goal of this work is to propose a mechanism for the formation of coke during the HDO of raw bio-oil. For this reason, further studies on the location and nature of the carbonaceous species deposited on an activated carbon-based Pt-Pd catalyst have been carried out. Several *post-mortem* analyses (N_2 adsorption-desorption, temperature-programmed oxidation (TPO), laser desorption ionization/mass spectrometry (LDI/MS) and FTIR spectroscopy) of catalysts used at different temperatures in a fixed bed reactor and of the deposited coke have been used for this purpose.

2. Experimental

2.1. Catalysts preparation

The activated carbon support was prepared from olive stone (OS) through chemical activation with H_3PO_4 (3 g H_3PO_4 per g OS). The impregnated precursor was dried at 100 °C and carbonized at 500 °C in N_2 (150 $cm^3\,min^{-1}$) for 2 h. The support was washed with distilled water until constant or neutral pH was reached in the eluent, and then it was dried and sieved to the desired particle size (100–300 μm). Pt and Pd were simultaneously incorporated through incipient wetting impregnation, with an aqueous solution of $HPtCl_6{\cdot}6HCl$ and $PdCl_2$ slightly acidified with HCl, in order to achieve a nominal value of Pt and Pd of 1 wt% and of 0.5 wt%, respectively. The catalyst was finally heat-treated at 400 °C for 4 h in N_2. Further information about the preparation method can be found elsewhere [37].

For the sake of comparison, a Pt-Pd supported on a discarded fluid catalytic cracking (FCC) catalyst (used as a support) was prepared. The industrial FCC support was tableted and sieved to the same particle size (100–300 μm) and the catalyst was prepared by impregnation method at pH = 7 using solutions of $Pt(NH_3)_4(NO_3)_2$ and $Pd(NH_3)_4(NO_3)_2$ as metal precursors, followed by water removal at 80 °C in vacuum. The bifunctional catalyst was dried at 100 °C and calcined at 500 °C for 3 h. A FCC-based catalyst has been previously used for hydroprocessing light cycle oil (LCO), showing high activity as a consequence of: (i) the mesoporous texture of the FCC support, and; (ii) the high dispersion of metal nanoparticles [61]. Both catalysts were designated as their corresponding support (ACP and FCC).

2.2. Bio-oil and liquid product characterization

The raw bio-oil was obtained through fast pyrolysis of black poplar sawdust at 450 °C in a pilot plant with a capacity of 25 $kg\,h^{-1}$, provided with a conical spouted bed reactor [62]. After the HDO runs, the obtained liquid products were separated into oxygenate and hydrocarbon fractions, mainly composed of oxygenated molecules and hydrocarbons, respectively [37]. The raw bio-oil and these oxygenates, and hydrocarbons were characterized by means of gas chromatography. On the one hand, the composition of the bio-oil and the oxygenate fraction was determined using a gas chromatograph provided with a BPX5 column (length, 50 m; internal diameter, 0.22 mm), and coupled on-line with a mass spectrometer (Shimadzu GC/MS QP2010). On the other hand, the hydrocarbon fraction was characterized by means of comprehensive chromatography (GC × GC) provided with two columns of different polarity connected by a flow modulator and a FID detector. The first column was a non-polar DB-5MS (length, 30 m; internal diameter, 0.25 mm), and the second one was a polar TRB-50 HT (length, 5 m; internal diameter, 0.25 mm). The GC × GC Agilent 7890 A chromatograph was also coupled with a mass spectrometer (MS) Agilent 5975C.

Further information on the composition of the liquids was obtained by means of *ex-situ* FTIR spectroscopy using a Nicolet 6700 apparatus. A droplet of the liquid (bio-oil and both product fractions) was sandwiched in between two tablets of KBr (100 mg) and placed into the transmission cell. Spectra were recorded using 60 scans and a resolution of 4 cm^{-1}. Moreover, the water content in the bio-oil and liquid products was measured by Karl-Fischer titration, using a Metrohm 830 K F Titrino plus apparatus.

In order to facilitate the understanding of the chromatographic results the compositions of the liquid products were expressed in terms of double bond equivalent values (DBE). DBE represents the degree of unsaturation (or aromaticity) of the compounds and it was depicted as a function of the number of carbon atoms, which represents the degree of alkylation of the molecule. This representation is used with the objective of finding a relation between the compositions of liquid products (containingcoke precursors) and the species retained in the used catalysts (coke). This analysis based on DBE is extendedly applied in the characterization of petroleum oils [63] and bio-oil [64,65]. DBE is determined as:

$$DBE = c + 1 - \frac{h}{2} \quad (1)$$

where c and h are the number of carbon and hydrogen atoms of each molecule, respectively. For example, according to this equation, a molecule as acetic acid presents a DBE of 1 whereas phenol has a DBE of 4.

Fig. 1 shows the results of bio-oil composition, in terms of DBE as a function of the number of carbons of the molecule. These results were obtained from the integration of the GC/MS chromatograph of Figure S1a in the Supporting Information. Well-defined and highly intense peaks are observed in the chromatogram for the main compounds of bio-oil [37]: acetic acid (23.5 wt%), hydroxyacetone (7.2 wt%), phenol (3.5 wt%) and levoglucosan (24 wt%). The range of carbon length includes short chain oxygenated molecules, such as acetic acid, and

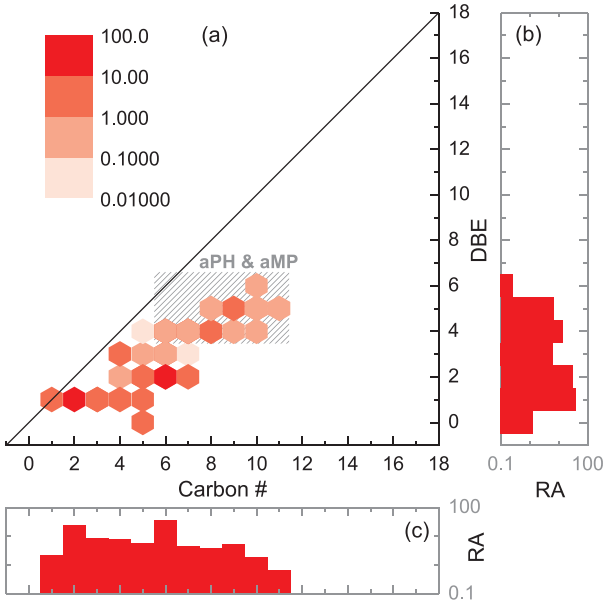

Fig. 1. (a) Contour map of DBE versus the number of carbons for the raw bio-oil (Color intensity referred to the relative abundance of each lump of compounds), and (b) DBE and (c) number of carbons versus their relative abundance (RA).

Table 1
Most representative compounds of bio-oil from black poplar sawdust.

Name	Peak number	Carbon #	DBE
Methanol	1	1	0
Acetone	2	3	1
Acetic acid	3	2	1
Hydroxyacetone	4	3	1
Ethanol	5	2	0
Furanone	6	4	3
Phenol	7	6	4
Methyl phenols	8, 9	7	4
3-Methyl-1,2-cyclopentanedione	10	6	3
Cyclopropylcarbinol	11	4	1
Syringol	12	8	4
Apocynin	13	8	5
Levoglucosan	14	6	2
Syringaldehyde	15	9	5

heavier polysubstituted-phenols as syringol, apocynin and syringaldehyde. The most representative compounds of bio-oil are listed in Table 1, where the number of carbon atoms and the DBE values of each molecule are detailed. The main fraction of compounds exhibits values of DBE = 1–3 (ca. 78 wt%). Cyclopropylcarbinol, furanone and 3-methyl-1,2-cyclopentanedione are included in this group of molecules (Figure S1a). On the other hand, unsaturated compounds of DBE > 4 are also identified. These molecules with aromatic rings, unsaturated alkyl substituents and more than one oxygen atom have been reported as the main responsible for catalyst deactivation due to their tendency towards repolymerizing and forming lignin-like solid deposits on the catalyst pores [58,66]. Hence, they have been grouped in the lumps of alkyl phenols (aPH) and alkylmethoxy phenols (aMP), which are highlighted in Fig. 1. The fraction of aPH and aMP (DBE > 4) is of 20.5 wt% whereas the fraction of long chain oxygenates (C_{6+}) accounts for 52.7 wt%.

2.3. HDO runs

Bio-oil hydrodeoxygenation (HDO) runs were carried out in a previously described [37] fixed bed reactor using the following experimental conditions: 400–450 °C, 65 bar, space time, 0.18 g_{cat} h $g^{-1}_{bio\text{-}oil}$; H_2:bio-oil volumetric ratio, 2000 cm^3_{H2} (STP) $cm^{-3}_{bio\text{-}oil}$; time on stream, 0–8 h. At these conditions, theoretical studies based on the Thiele module and the Weisz-Prater criterion indicate that the main oxygenates in bio-oil do not show diffusion limitations. Gas products were analyzed on-line in a Varian CP-4900 microGC, whereas liquid ones were sampled at 1 h intervals and analyzed as described in the previous section. The carbon balance closed up to ca. 90 %, which is attributed to the difficulties for measuring the exact amount of coke on the carbon-based catalyst. In order to study the evolution of the reaction with time on stream, a HDO conversion (X_{HDO}) was defined as a function of the water content in the bio-oil and in the products:

$$X_{HDO} = \frac{F_w|_{prod} - F_w|_{bio-oil}}{F_w|_{theoretical}} 100 \quad (2)$$

where $F_w|_{prod}$ and $F_w|_{bio\text{-}oil}$ are the mass flow of water in the liquid product and in the fed bio-oil (determined by Karl-Fischer titration), respectively, and $F_w|_{theoretical}$ is the theoretical maximum mass flow of water that can be obtained by hydrodeoxygenation of the organic compounds of raw bio-oil, i.e. excluding water contained in the bio-oil.

2.4. Used catalyst characterization

The porous texture of the catalysts was studied by means of N_2 adsorption-desorption at -196 °C, using a Micromeritics ASAP2020 apparatus. Catalysts were degassed at 150 °C for 8 h prior to analysis to remove impurities. From N_2 isotherms, specific surface area (S_{BET}) was determined using the Brunauer-Emmett-Teller equation, whereas micropore volume (V_{mic}) was determined with the *t*-plot method, based on the Harkins-Jura equation. Mesopore volume (V_{mes}) was calculated as the difference between total pore volume ($V_{0.995}$) and micropore volume.

Used catalysts were characterized through thermogravimetric analyses of temperature-programmed oxidation (TG-TPO). Samples were firstly submitted to a stripping treatment in N_2 at the reaction temperature (rising the temperature at 10 °C min^{-1}) in order to sweep the reactants adsorbed on the catalyst surface. Afterwards, they were subjected to a continuous air flow (50 cm^3 min^{-1}), raising the temperature up to 900 °C at a heating rate of 5 °C min^{-1}.

The nature of the species deposited on the catalyst was analyzed by Laser Desorption-Ionization and mass spectroscopy (LDI/MS). LDI/MS measurements were carried out on a Bruker Autoflex Speed instrument equipped with a 355 nm Nd:YAG laser. All spectra were acquired in the positive-ion reflectron mode (accelerating voltage, 20 kV; pressure, $5{\cdot}10^{-6}$ mbar). Each sample was immerged in an acetonitrile solution (1% trifluoroacetic acid) and prepared according to the "dry droplet" method using a polished steel target. LDI analyses were carried out without using any matrix because of the high intensity of the matrix peaks, which might distort the results [67].

The surface of used catalysts was also characterized by means of FTIR spectroscopy. Samples of used catalyst were pelletized with KBr (200 mg) and then introduced in a transmission cell, which was placed inside a Specac catalytic chamber. The catalytic chamber was connected on-line with the previously described Nicolet 6700 apparatus. Experiments were carried out up to 105 °C raising the temperature at a heating rate of 5 °C min^{-1} in order to assure the removal of water in solid samples. From the collected data, several FTIR bands were identified and integrated [68–70]: 1260 cm^{-1} (C–O stretching in aromatics), 1450 cm^{-1} (C–O stretching in COH and C–H stretching in aliphatics and alkyl aromatics), 1530–1680 cm^{-1} (C=C stretching in aromatics), 1700 cm^{-1} (C=O stretching), 2800–3000 cm^{-1} (C–H stretching in aliphatic), 3000–3150 cm^{-1} (C–H stretching in aromatics) and 3200–3600 cm^{-1} (O–H stretching).

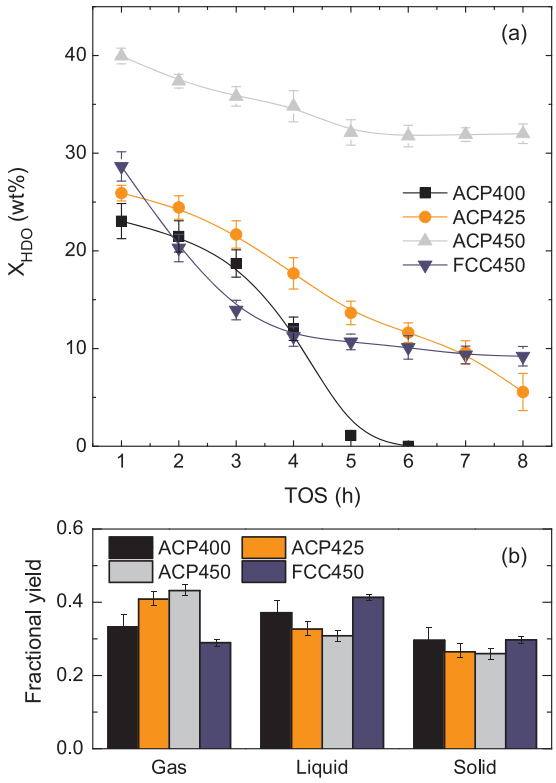

Fig. 2. (a) Evolution of the HDO conversion with time on stream and (b) product fraction distribution for the different catalysts and conditions (experimental error bars have been estimated from data obtained in 2 to 3 experiments).

3. Results

3.1. Evolution of the conversion and composition

Fig. 2a shows the evolution of the HDO conversion (X_{HDO}), calculated from the Eq. (2), with the time on stream (TOS) for the ACP catalyst at 400, 425 and 450 °C (ACP400, ACP425 and ACP450 runs, respectively) and for the FCC catalyst at 450 °C (FCC450 run). Both catalysts exhibit a decrease in X_{HDO} during the initial 6 h of time on stream, nonetheless the drop of the conversion is milder when the reaction temperature is increased, and at 450 °C (ACP450 and FCC450 runs) a pseudo-steady HDO conversion is observed after 5 h in both cases. This performance has been attributed to the similar rates of the formation of deactivating species and of the hydrocracking of their precursors [37]. However, a higher X_{HDO} is observed when using the ACP catalyst, suggesting that the porous texture of the activated carbon and their phosphorus and oxygen surface functional groups favor the mechanisms of bio-oil HDO. On the other hand, the ACP catalyst exhibits null X_{HDO} after 5 h at 400 °C, when the blockage of the reactor was caused by a massive deposition of carbonaceous species on the catalytic bed.

Fig. 2b depicts the total amounts of gaseous, liquid and solid fractions obtained as products of HDO runs for each catalyst and temperature. As a consequence of the cracking of hydrocarbons, the gaseous fraction is higher upon increasing the temperature, which leads to a decrease in the liquid fraction. The slightly higher acidity of ACP also favors the production of gaseous products through cracking, decarbonylation and decarboxylation pathways. The solid fraction is similar for the four HDO runs, observing a slight drop when the temperature is raised. The higher yield of solid fraction for the FCC catalyst could be attributed to an easy retention of big oxygenated compounds in the matrix of the catalyst. Compared to a recently reported two-stage HDO process, the obtained liquid fraction yields are lower, whereas the yields of gas and solid fractions increase [31]. This is associated with the higher HDO temperature required for reaching the pseudo-steady state observed in Fig. 2a.

HDO runs were also monitored through *ex-situ* FTIR spectroscopy, analyzing the evolution of the different bands of liquid products with TOS. Figure S2 shows the FTIR spectra of the raw bio-oil and the liquid products at TOS = 1 and 8 h obtained with the ACP (Figure S2a) and FCC (Figure S2b) catalysts at 450 °C. Bio-oil shows a similar spectrum than those previously reported by several authors [71–73]. Intense bands are observed at 1700 and 3200–3600 cm^{-1}, which are attributed to ketone-type (C═O) and hydroxyl (O—H) species, respectively (present in levoglucosan, acetic acid or ketones, which also vibrate at the 2850, 2930 and 2960 cm^{-1} aliphatic bands). Moreover, the presence of bands at 1260, 1530 and 1620 cm^{-1} is explained by the aforementioned aPH and aMP compounds (see Fig. 1). After 1 h of reaction at 450 °C using the ACP catalyst, the spectrum observed for the liquid product only shows two well-defined bands (Figure S2a), attributed to water (band at 3450 cm^{-1} of O—H bond) and unsaturated aldehydes or ketones (band at 1680 cm^{-1}) [74]. The absence of bands at 1530 and 1260 cm^{-1} suggests that phenolic compounds are completely transformed at TOS = 1 h. This band and a shoulder at ca. 3100 cm^{-1} can be observed after 1 h when using the FCC catalyst (Figure S2b), confirming the lower X_{HDO} registered for this catalyst (Fig. 2a).

The increase in the relative intensity of oxygenated bands (1260 and 1700 cm^{-1}) with TOS (Figure S3a) and the decrease in the one attributed to water (3200–3600 cm^{-1}) are due to the drop of X_{HDO} caused by catalyst deactivation. Two phases are separated in the liquid product after 4 and 6 h of reaction for ACP and FCC catalysts, respectively. The oxygenate fraction shows a similar spectrum than that registered at 1 h, but the bands at 1260 and ca. 3100 cm^{-1} are observed for both catalysts (more intense in the FCC450 run, Figure S2). The intensity of oxygenated and aromatic bands suffers a pronounced decrease at TOS = 6 h (Figure S3a), when a portion of oxygenated compounds, as ketones and phenols, are transferred to the hydrocarbon fraction. At this point of the reaction, the presence of high amounts of water and non-polar 2- or 3-ring aromatics in the reaction medium leads to a phase separation. After that, the increase in aromatic compounds could be explained by the lower capability of the catalyst for hydrodeoxygenating phenols.

Many more defined bands are distinguished in the spectra of the hydrocarbon fraction at 8 h (Figure S2b). The bands at 1530, 1620, 3020 and 3150 cm^{-1} point out the presence of aromatic structures in this product fraction. The three main bands in the hydrocarbon fraction for the ACP450 run are the ones assigned to hydrodeoxygenated aliphatic chains (2800–3000 cm^{-1}). In addition, some oxygenated compounds can be identified, such as phenols (1260 cm^{-1} band), ketones (1700 cm^{-1} band) and alcohols (3450 cm^{-1} band), whose intensity is much higher for the FCC450 run. Regarding their evolution (Figure S3b), the drop of the intensity of aliphatic bands, together with the increase in the aromatic and oxygenated ones (1530–1680, 3000–3150 and 3200–3600 cm^{-1}), suggest that the formation of saturated compounds through aromatic hydrogenation is inhibited upon increasing the TOS for the ACP425 and FCC450 runs. However, the increase in the aliphatic band when using the ACP catalyst at 450 °C confirms the pseudo-steady X_{HDO} observed at these conditions and then, the equilibrium between the formation of polyaromatic deactivating species and the hydrocracking of their precursors [37].

In order to identify the main precursors of deactivating species and understand the most reasonable deactivation pathways, the composition of the reaction medium in the last hour of reaction are displayed in Figs. 3 and 4. The results have been calculated from the GC/MS chromatograms of the oxygenate fraction (Figure S1b) and the GC × GC/MS chromatograms of the hydrocarbon fraction (Figure S4). In this sense, Fig. 3 depicts the composition of the oxygenate fraction whereas the one of hydrocarbon fraction is displayed in Fig. 4. The absence of phase

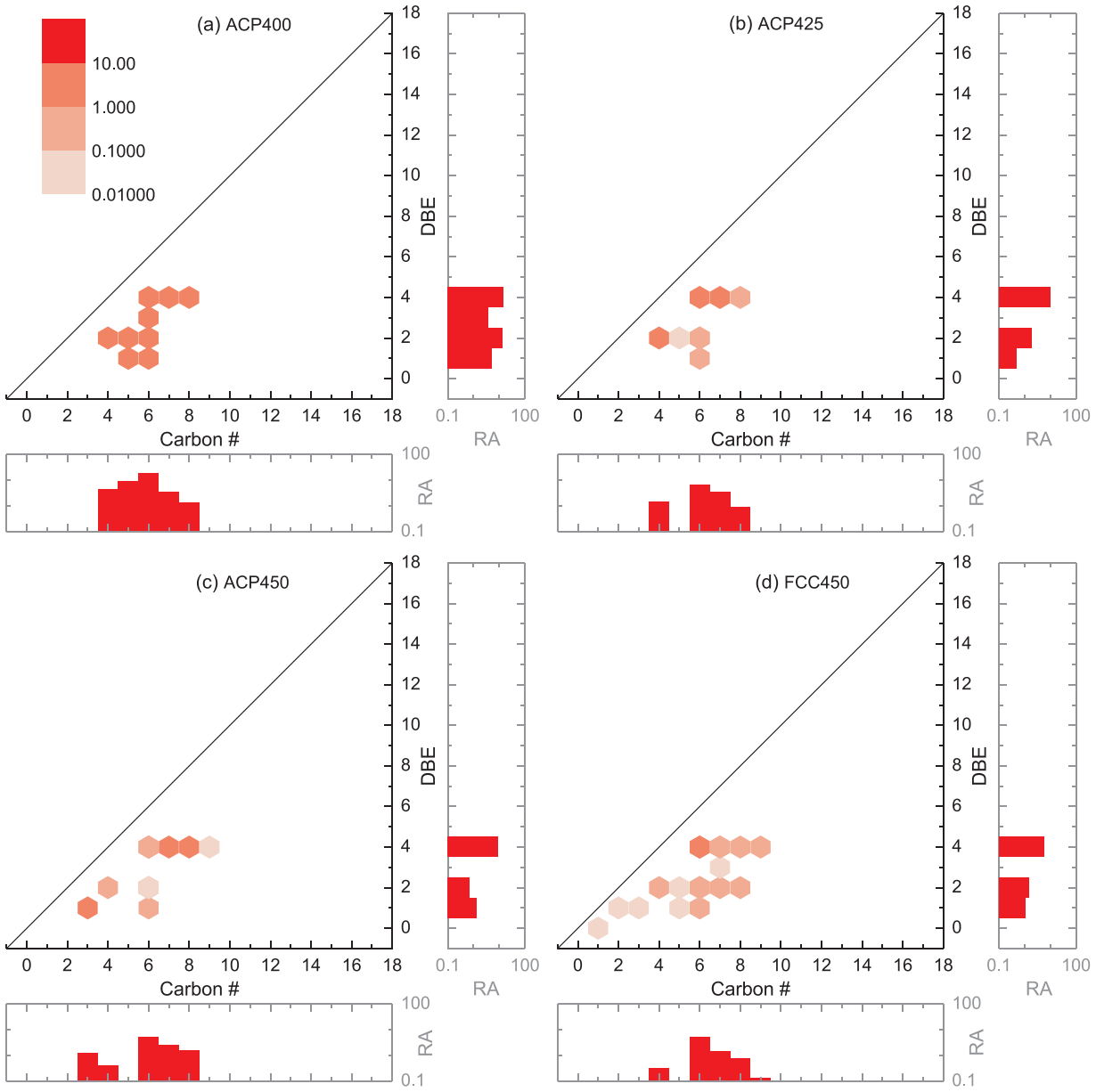

Fig. 3. Contour map of DBE versus the number of carbons, and DBE and number of carbons versus their relative abundance (RA), for the oxygenate fraction of the liquid product obtained with the ACP catalyst at (a) 400 °C, (b) 425 °C and (c) 450 °C, and (d) with the FCC catalyst at 450 °C. (Color intensity referred to the relative abundance of each lump of compounds).

separation at TOS = 6 h using the ACP catalyst at 400 °C is noteworthy. At these conditions, an emulsion liquid phase is observed in the products and it is mainly composed of water and oxygenated hydrocarbons. Even though methanol (DBE = 0) present the highest concentration in the oxygenate fraction for all catalysts and HDO temperatures [37], it is not included in the results of Fig. 3 because its intensity distorts the results and avoids a clear interpretation of data.

Regarding the composition of the oxygenate fraction obtained with the ACP catalyst, three families of oxygenated compounds are identified according to DBE values: linear (DBE = 1; ketones and carboxylic acids), cyclic (DBE = 2; furanones, cyclopentanones and cyclohexanones) and alkylphenols (aPH, DBE = 4). The increase in HDO temperature leads to an advance in the HDO reaction, which decreases the total amount of oxygenated molecules in the reaction medium (from 37.1 wt% at 400 °C to 11.1 wt% at 450 °C, Fig. 3). Additionally, an increase in the fraction of oxygenated compounds with DBE = 1 is registered comparing the HDO runs at 425 and 450 °C (0.5 and 1.4 wt%, respectively). On the other hand, the lower X_{HDO} with FCC catalyst increases the variety of oxygenated molecules with DBE = 1–2 (Fig. 3d), observing chains from 2 (acetaldehyde) to 8 (ethylcyclohexanone) carbon atoms. Moreover, the presence of molecules with DBE = 3 (ACP400 and FCC450, Fig. 3a and d) points out the higher concentration of partially hydrodeoxygenated compounds at these low X_{HDO} values (Fig. 2a).

These results are in good concordance with those registered for the hydrocarbon fraction (Fig. 4). In this case, compounds have been grouped in: paraffins and iso-paraffins (PF, DBE = 1), alkyl naphthenes (aNP, DBE = 2), 1-ring alkyl aromatics (aA1, DBE = 4–6), 2-ring alkyl aromatics (aA2, DBE = 7–9) and 3-ring alkyl aromatics (aA3, DBE = 10). The higher hydrocarbon fraction yield obtained with the ACP catalyst at 450 °C (20.5 wt%) (Fig. 4c) in contrast to that at 425 °C (17.3 wt%, Fig. 4b) and with the FCC catalyst (13.9 wt%, Fig. 4d) should be highlighted. Furthermore, an increase in the concentration of aA2 and aA3 is observed upon increasing the temperature from 425 to

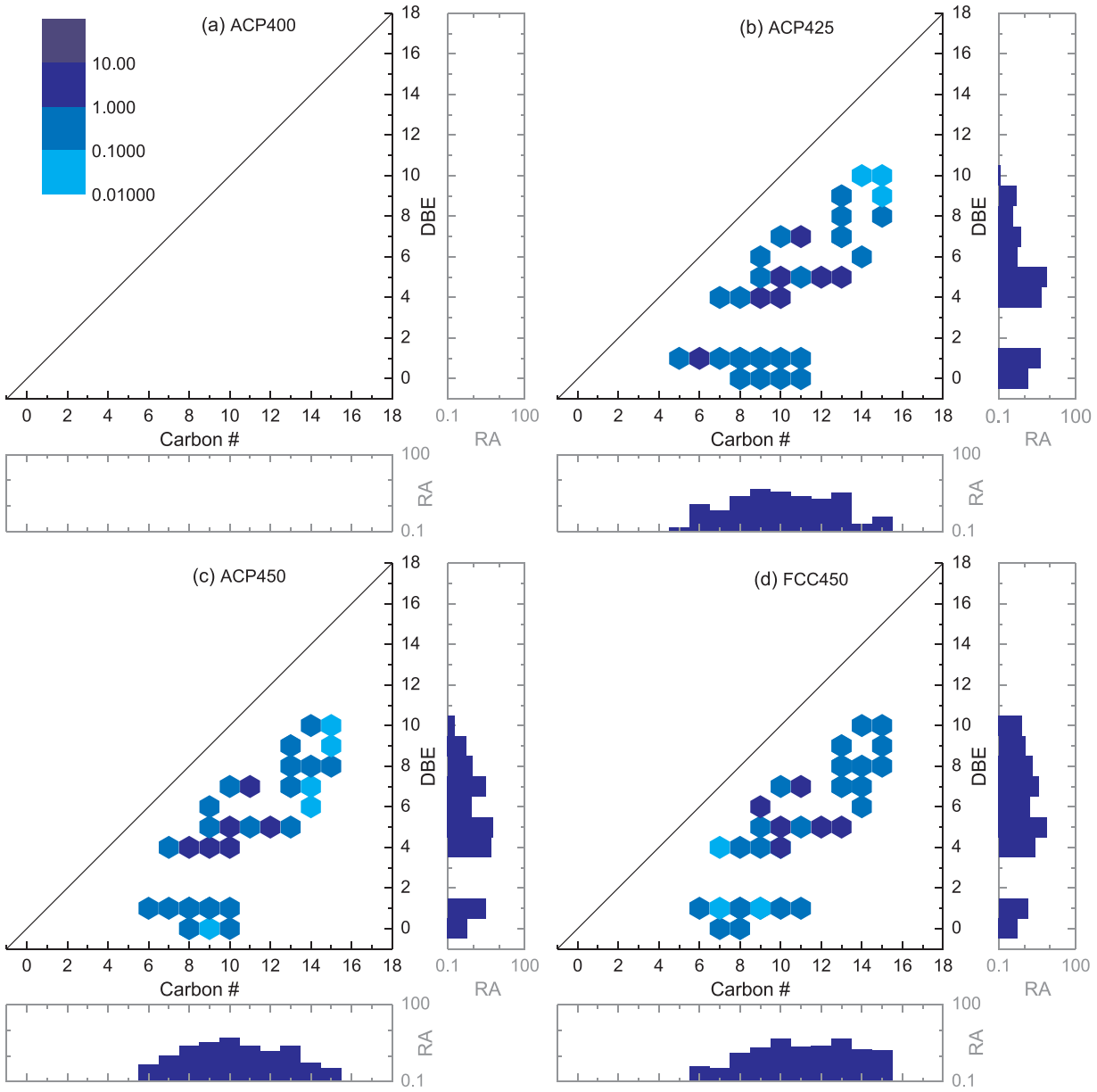

Fig. 4. Contour map of DBE versus the number of carbons, and DBE and number of carbons versus their relative abundance (RA), for the hydrocarbon fraction of the liquid product obtained with the ACP catalyst at (a) 400 °C, (b) 425 °C and (c) 450 °C, and (d) with the FCC catalyst at 450 °C. (Color intensity referred to the relative abundance of each lump of compounds).

450 °C (1.7 and 4.8 wt%, respectively, Figs. 4b and c). On the contrary, the concentration of PF and aNP decreases from 5.8 to 3.5 wt% when the HDO temperature is raised. This suggests that the hydrogenation of aromatic rings is favored at low HDO temperatures. In terms of number of carbon atoms, average chain lengths of 9 (425 °C) and 10 (450 °C) carbon atoms are registered using the ACP catalyst, which indicates that an increase in the temperature promotes the aromatization and condensation of carbon structures towards coke. The FCC catalyst yields an average carbon chain length of 12 and presents higher concentration of aA2 and aA3 than the ACP one at 450 °C (Fig. 4d). This greater ability of FCC catalyst to condense the carbon structures could be attributed to an enhanced formation of bigger molecules (precursors of coke) within its macroporous matrix. Therefore, this different composition of the reaction medium would explain the more pronounced deactivation by coke of the FCC catalyst at the same HDO temperature (Fig. 2a).

According to the aforementioned results, a hypothesis of a deactivation mechanism based on the two different precursors of carbonaceous coke species (identified in the reaction medium) could be stated: phenolic molecules (aPh and aMP, in the oxygenate fraction) and alkyl polyaromatics (aA2 and aA3, in the hydrocarbon fraction). Fig. 5 displays the relative concentration of each of these precursors in the last hour of reaction. Two marked trends are exhibited by each one in the oxygenate and hydrocarbon fractions. On the one hand, the concentration of aPh and heavy oxygenated molecules (C_{6+}) decreased when the HDO temperature was raised (ACP catalyst) while, on the other hand, aA2 and aA3 concentrations increase upon increasing the temperature, even though they remain significantly lower in contrast with oxygenated coke precursors. This is consistent with the favored oxygen removal [15] and aromatization/condensation of organic molecules [46] observed at high temperatures in hydroprocessing reactions. Therefore, HDO temperature plays a key role in the composition of reaction medium and thus, in the origin of carbonaceous deposits. In addition, the catalyst support has also a marked effect on the reaction medium composition, and higher concentrations of oxygenated and

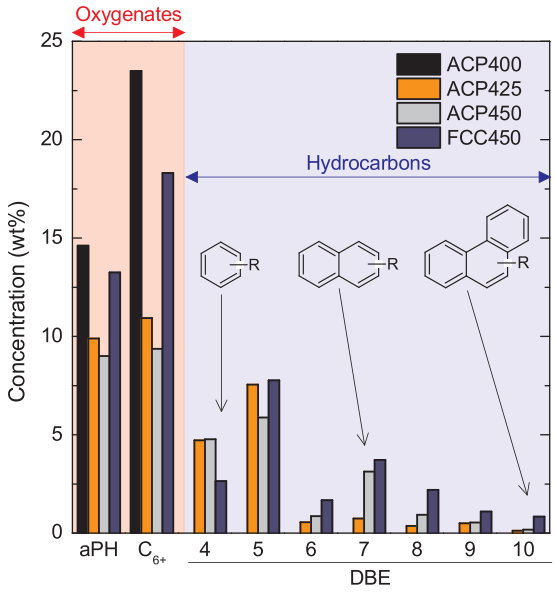

Fig. 5. Distribution of representative products in the oxygenate and hydrocarbon fractions using ACP and FCC catalysts at 400–450 °C.

organic precursors are observed with the FCC catalyst at 450 °C.

3.2. Location of deactivating species on the porous texture of the catalyst

The deposition of the carbonaceous species on the catalyst surface leads to a deterioration of its physico-chemical properties and in the worst case scenario, to the reactor blockage (clogging). Fig. 6 displays the decrease in the specific surface area (S_{BET}), total pore volume ($V_{0.995}$), micropore volume (V_{mic}) and mesopore volume (V_{mes}) of the used catalysts after the HDO runs. The used catalysts were named using the same nomenclature that the run in which they were used. Used ACP catalysts exhibit a drop of the surface area higher than 75% of its initial value (1305 $m^2 g^{-1}$, Fig. 6a). Moreover, some differences are observed for each used ACP catalyst regarding the effect of the temperature on the blockage of the pores. The ACP400 catalyst exhibits the largest surface area (and the lowest deterioration) despite it shows the more pronounced activity loss with time on stream (Fig. 2a). The values of micropore and mesopore volumes for the three used catalysts denote two different effects of deposited carbonaceous species on the deterioration of the surface properties. On the one hand, ACP400 catalyst shows a remarkably higher V_{mic} (0.26 $cm^3 g^{-1}$) than ACP425 and ACP450 catalysts (ca. 0.02 $cm^3 g^{-1}$). On the other hand, it shows much lower V_{mes} than the catalysts used at higher temperatures. This result suggests that the deposition of carbonaceous species on the mesopores of the catalyst is favored at lower HDO temperatures, whereas higher HDO temperatures favor the deposition of carbonaceous species on the active sites within the micropores of the catalyst. This location, together with a high HDO temperature, allows for partially hydrocraking the precursors of coke and achieving the pseudo-steady state previously observed in Fig. 2a. In correlation with Fig. 6a, the deposition on the mesopores causes a faster catalyst deactivation and, as the catalytic activity drops, the concentration of the deactivating precursors increases, triggering an even faster or autocatalytic deposition that ultimately leads to the blockage of the reactor. On the other hand, the carbonaceous species deposited at temperatures higher than 425 °C deteriorate the micropores to a greater extent than mesopores, which has a lesser effect on catalyst deactivation. This is also noticeable regarding the textural properties of the FCC450 catalyst (Fig. 6b), which exhibits a complete micropore (V_{mic}) blockage, but also reaches the pseudo-steady HDO conversion state after 4 h (Fig. 2b).

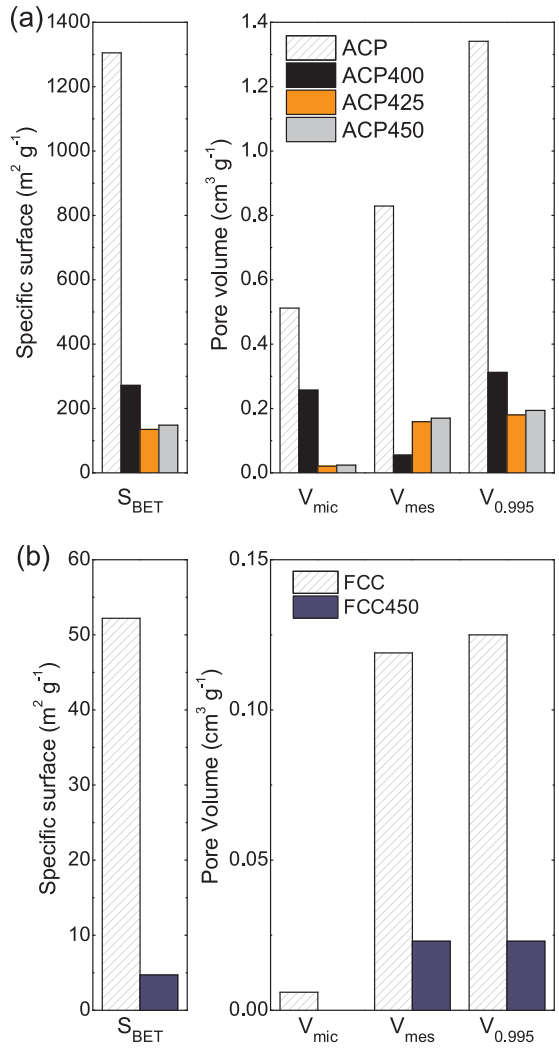

Fig. 6. Deterioration of the main textural properties for the used (a) ACP catalyst at 400–450 °C and (b) FCC catalyst at 450 °C.

3.3. Nature of deactivating species

TPO profiles of the used catalysts provide further information about the location and nature of the deactivating species. Fig. 7a shows those TPO profiles, visualizing two main combustion zones, associated with the deactivating species and the carbon support, respectively. At the same time, two combustion zones are observed within the region for deactivating species themselves, one corresponding to thermal or pyrolitic lignin (TL) and another one for coke (CK, presumably with a catalytic origin). In order to reinforce these assignments, TPO experiments of the bare ACP support and the bare TL were carried out. In previous works, the nature of the TL deposited on different catalysts and conditions was ascribed to repolymerized phenols of the bio-oil [28,37,75]. Thus, a practical approach to quench this deposition is using a thermal treatment (before the catalytic reaction) at no less than 400 °C in a U-shaped stainless steel tube [68]. The TPO of the bare TL obtained in this thermal treatment is shown in Fig. 7b and only one defined peak is observed at ca. 425 °C. Otherwise, Fig. 7b also shows that the combustion of the bare ACP support occurs within the range of 500–600 °C. These results are consistent with the assignments of the different TPO peaks. Finally, the assignation of the second peak of Fig. 7a to catalytic coke (CK) is supported by previous results of coke formation during the conversion of bio-oil into olefins over a HZSM-5 zeolite [75].

Then, it is possible to observe in Fig. 7a that the amount of TL is

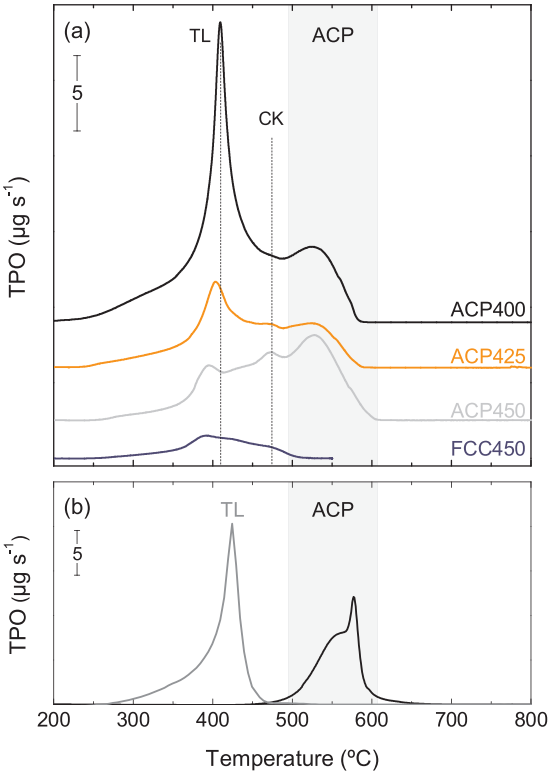

Fig. 7. TPO profiles of the (a) used ACP and FCC catalysts, (b) the fresh ACP catalyst and the bare thermal lignin (TL).

greater for the ACP catalysts and when the temperature is lowered. Moreover, the intermediate peak at ca. 470 °C assigned to CK is observed for all the catalysts and increases with temperature. We might well expect a certain degree of overlapping between the deactivating species and the ACP support, as it was previously reported [46]. These results (Fig. 7) together with the previous ones (Figs. 2 and 6) indicate that the TL is deposited on the mesopores of the catalyst, causing severe deactivation since it hinders the access of the reactant to the active sites (mainly located in the micropores). On the contrary, CK is mainly deposited in the micropores of the catalysts or their entrances, blocking the active sites but causing a less severe deactivation. Moreover, this deactivation can be partially controlled by using a HDO temperature of 450 °C, which favors the HDO of oxygenated compounds and the partial cracking of coke precursors. The FCC450 catalyst, with a very different porous texture, shows less defined peaks in the TPO profile, suggesting the presence of more heterogeneous carbonaceous deposits (formed by TL and CK) mainly located in the mesopores of the support (Fig. 6b). According to the different acid properties of both supports [37], the differences in the nature of the coke deposited at the same temperature in both catalysts could also be attributed to faster mechanisms of carbonaceous species condensation over the stronger acidic sites of ACP.

The temperature of combustion of TL and CK can be associated with its location, as it has been discussed, but also with a different nature [46]. In such a way, the low temperature of combustion of TL species corresponds to a little developed structure, located on the mesopores and on the external surface of the catalyst. On the other hand, CK burns off at high temperatures, which is related to its more condensed nature and a location on the micropores (where the combustion has more diffusion limitations). TL is presumably formed from bio-oil oxygenates, which explains its location on the external surface or on the mesopores of the catalyst, while CK likely evolves from the hydrocarbon intermediates that diffuse towards the micropores of the catalyst, where they condense following a mechanism promoted by the acidic sites.

The growth of both CK and TL will have a direct effect on bio-oil hydrodeoxygenation activity, as the diffusion times of reactants towards the active sites will increase greatly. Thus, we may well expect diffusion limitations at long times on stream. However, coke formation would not be limited in the same manner, and parallel homogeneous reactions will occur, in particular those that build up TL on the catalytic surface. That is, the overall deactivation mechanism will remain the same but certain reactions would be favored by increased diffusion resistances.

Considering the previous results of TL deposition in the absence of a catalyst [68], we might well explain the origin of TL as thermal reactions of polymerization of phenols on the surface of the catalysts. If these phenols are not converted by the catalyst, they keep depositing even with a completely deactivated catalyst, leading to reactor blockage. Furthermore, TL species have a partially developed microporous texture, which is suggested by the higher values of V_{mic} observed for ACP400 catalyst in comparison to those for ACP425 and ACP450 catalysts (Fig. 6a). Otherwise, the origin of CK (TPO peak at 470 °C) is presumably catalytic, since its formation is a consequence of the condensation of certain precursors on the metallic or acidic sites of the catalyst [55]. At HDO temperatures of 450 °C, the formation of TL and CK is equalized by the hydrocracking of their precursors, reaching a pseudo-steady HDO conversion observed in Fig. 2a for the ACP450 run. On the other hand, the rate of TL and CK formation is higher than that of the hydrocracking of their precursors at 425 °C, which leads to a more severe catalyst deactivation (ACP425 run in Fig. 2a).

The nature of the ACP catalyst and the carbonaceous species deposited during the reaction was also analyzed by means of LDI/MS spectroscopy. Fig. 8a shows the mass spectra obtained for the fresh ACP catalyst and the ACP450 catalyst and Fig. 8b illustrates the overall normalized distribution of all the used catalysts. The fresh catalyst exhibits a very neat spectrum with several well-defined peaks at some specific mass values (393, 409, 450, 465, 684 and 702 Da), whose intensity is relatively low. The ACP450 catalyst has a wide number of peaks along the 200–1000 Da range, each separated by 1 Da. This result indicates the presence of a wide variety of deactivating species (not observed in the bare support) trapped within the pores of the catalyst. The maximum intensity of the LDI/MS spectrum for ACP450 catalyst is observed at ca. 642 Da, which indicates that this is the most likely mass of the deposited species. Normalized distribution of LDI/MS spectra of the different used catalysts are also shown in Fig. 8b. The maximum of the normalized distribution for the ACP400 catalyst is observed at lower masses (ca. 552 Da) than those for the ACP425 and ACP450 catalysts. This could be due to the lower weight of the structures

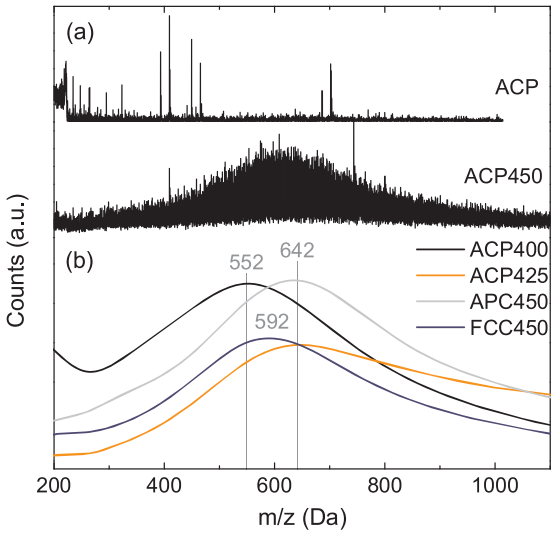

Fig. 8. (a) LDI/MS spectra of the fresh and the used ACP catalyst at 450 °C, and (b) normalized distribution of the LDI/MS profiles of the used catalysts.

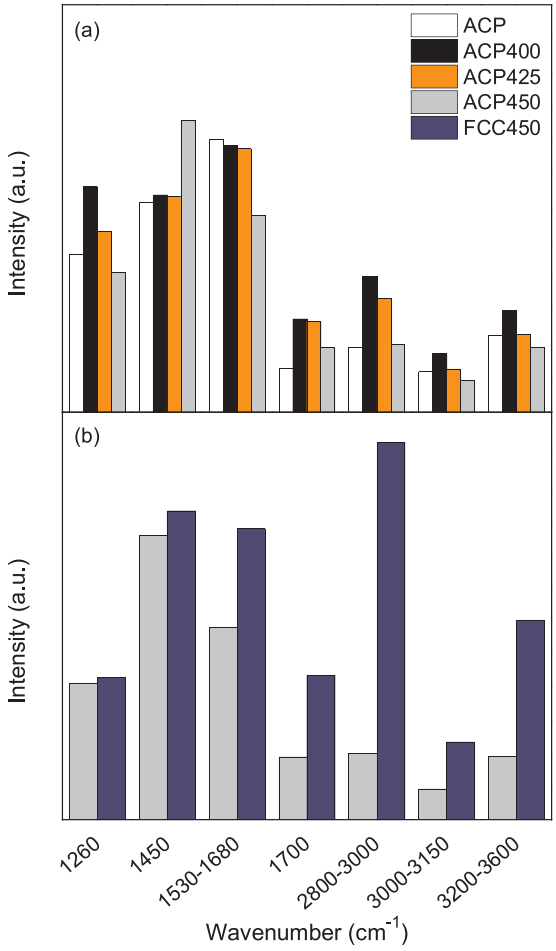

Fig. 9. Intensity of the FTIR bands obtained from the integration of the spectra for the (a) used ACP catalysts at 400–450 °C and (b) the used ACP and FCC catalysts at 450 °C.

desorbed from the TL, being TL the main deposited species on the surface of the ACP400 catalyst. Moreover, the LDI/MS spectrum of FCC450 catalyst shows a shift of the maximum toward lower masses (ca. 592 Da) compared to that of the ACP450 catalyst. The higher acidity of the ACP catalyst [37] could explain this result, since it allows for the formation of more developed coke structures, thus yielding heavier species.

In addition, the composition of the carbonaceous species was analyzed by means of FTIR spectroscopy of the used catalysts. Fig. 9 displays the intensity of the main bands obtained for the different used catalysts. Because of the similar nature of the activated carbon support with that of deposited species, the same experiment was carried out with the fresh catalyst (Figure S5 in the Supporting Information shows the FTIR spectrum of the fresh and used catalysts at 450 °C). As observed, the main bands associated to the support are 1530–1680 and 1260 cm^{-1}, attributed to aromatic and phenolic (C—O bond in aromatics) species, which is in concordance with the structure of this P-containing activated carbon [41]. Comparing the ACP catalysts used at different temperatures (Fig. 9a), the decrease in the intensity of the oxygenated bands (1260, 1700 and 3200–3600 cm^{-1}) upon increasing the reaction temperature is noteworthy. This suggests a major presence of oxygen in the ACP400 catalyst, which confirms that the deposited species at this low temperature are mainly formed by TL (a polymer with O functionalities). Similar behavior is exhibited by the 2800–3000 cm^{-1} band (aliphatic compounds), indicating that the coke deposited at higher temperature shows a more developed structure, as was observed in Fig. 8a and in our previous work [37].

The differences in the kinetic behavior (Fig. 2a) and in the TPO profiles (Fig. 7) shown by the ACP450 and the FCC450 catalysts are also highlighted regarding the composition of the deposited species (Fig. 9b). The most significant difference between both catalysts is the high intensity of the 2800–3000 cm^{-1} band (assigned to aliphatic compounds) in the FCC450 catalyst. This result suggests a more amorphous and heterogeneous nature of the species deposited in the FCC450 catalyst and is consistent with the absence of defined peaks in its TPO profile (Fig. 7a) and the displacement of the maximum in the LDI/MS spectrum (Fig. 8a). In addition, the 1700 and 3200–3600 cm^{-1} bands also show a higher intensity in the FCC450 catalyst, being their intensity higher than that of phenolic compounds (1260 cm^{-1}). This way, the presence of oxygenated groups could be related to O-containing aliphatic structures

4. Discussion

Several works have been reported on the catalytic hydrodeoxygenation of bio-oil or its model compounds in the last few years [50–57], also indicating the most likely causes of deactivation and the main precursors of coke [58,60]. Fig. 10 shows the unified reaction and deactivation mechanism proposed for the HDO of bio-oil components, agglutinating mechanisms of the literature with the results obtained in this work. Acetone (KT), acetic acid (AC) and phenols (PH), which are three of the main compounds of this black poplar bio-oil, react relatively rapidly yielding short chain paraffins (PF) as ethane or propane. These PF are observed in the gaseous reaction products as LPG (liquefied petroleum gas) fraction [37]. The formation of LPG is reported to follow different routes as the direct hydrodeoxygenation of these reactants or the formation of 2-propanol (AL), the subsequent formation of an olefin (OL), and its final hydrogenation [8,44]. Sullivan and Bhan [50] reported the importance of both acidic and metallic sites of the bifunctional catalysts to accomplish this mechanistic route. Methanol is observed in great amounts in the oxygenate fraction of the product, which is mainly formed by the cleavage of a C—O bond of an ester (ET) [55]. These ET could be formed through the condensation of short oxygenated molecules, such as acetone (KT) or acetic acid (AC), as observed in Fig. 10 [44]. Moreover, several alkylmethoxy phenols (aMP) as guaiacol or anisole are present in the raw bio-oil (Figure S1), with relatively high concentrations (20.5 wt%), and suffer demethoxylation to form alkyl phenols (aPH) and methanol [56]. Apart from these routes, decarbonylation and decarboxylation routes are also noteworthy in the reaction scheme of HDO [44], since CH_4 and CO_x are also observed in the gaseous products [37]. The formation of CH_4 could also explain the registered ethane from acetone (via ethanol), apart from the proposed formation of methanol in Fig. 10 [8].

The HDO of aPH is widely studied in the literature as one of the most representative molecules of bio-oil. In this way, two main routes have been proposed: the cleavage of the C—O bond, yielding water and alkyl aromatics (aA1) through HDO route; and the scission of the C—C bond of the alkyl substituent (dealkylation) forming phenol, namely the hydrocracking route [7,51]. Additionally, direct hydrogenation of the aromatic ring of aA1 leads to the formation of alkyl cyclohexane following the first route. All these compounds are observed in the products of bio-oil HDO [37] as shown in Fig. 4. On the other hand, the formation of cyclohexane from phenol is commonly reported to follow a mechanism in which cyclohexanone, cyclohexanol and cyclohexene are intermediates [17,52–54,76]. Moreover, methylcyclopentane, which is other naphthenic compound observed (aNP), could be obtained from the recombination of cyclohexane molecules [76].

As it is also observed in Fig. 10, alkyl phenols (aPH) and single ring alkylated aromatics (aA1) are also formed through conjugation and condensation of dienes, which are intermediates in the mechanism of HDO of acetone and acetic acid. This was first reported by Furimsky [66], who explained the condensation of olefins over the acidic sites of the catalyst and that the organic fraction can be considered as a volatile

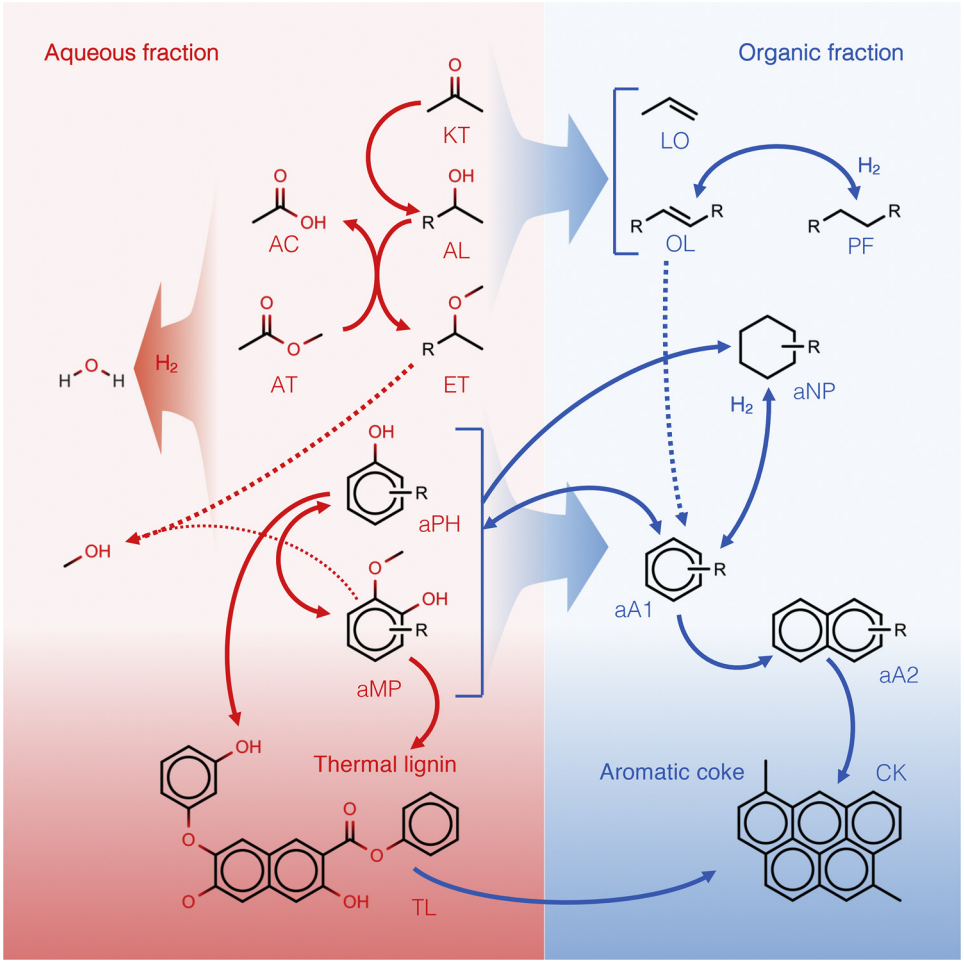

Fig. 10. Proposed mechanism for HDO of raw bio-oil including coke formation over the catalysts.

fraction of the deposits, and therefore it contains the main precursors of coke. Mortensen et al. [58] also reported the high tendency of alkene and aromatic compounds to form polyaromatic structures during HDO reactions. Indeed, we have also detected significant amounts of double- and triple-ring aromatics (aA2 and aA3, respectively) as shown in Fig. 5. These species can be conceived as aromatic coke (CK) precursors, which have also been identified in the catalytic pyrolysis of biomass using acid catalysts [33,34].

Thus, according to the literature and our results, two main deactivation pathways should be proposed in the reaction scheme of Fig. 10. The first one is the recombination of oxygenated compounds, which is faster at lower temperatures when the concentrations of alkyl phenols (aPH), alkylmethoxy phenols (aMP) and acetic acid (AC) are high due to a lower HDO conversion (Fig. 2a). The increase in the oxygenated compounds with time on stream observed in the aqueous fraction of the liquids (Figure S3a) explains the high amount of TL observed on the surface of the used ACP400 and ACP425 catalysts (Fig. 7). This rapid pathway leads to the deposition of lighter carbonaceous species (with oxygen-containing functionalities) on the external surface of the catalyst according to the characterization of the used catalysts (Figs. 6–8). The second pathway is the formation of polyaromatic structures through the condensation of the alkyl aromatics (aA1)into 2- and 3-ring aromatic structures, as observed in Fig. 5. The dehydrogenation of species is favored at higher temperatures and is promoted by the presence of intermediates as cyclohexene, which can react with aromatics in the acidic sites instead of forming cyclohexane (following the conventional HDO mechanism on the metallic sites). This second route explains the higher content of coke in the catalyst upon increasing HDO temperature (Fig. 7a), and the increase in the aromatic band of the organic fraction liquid products of ACP425 and FCC450 catalysts upon increasing the time on stream (Figure S3b). This route presents a catalytic origin (as it is activated by the metallic and acidic sites of the catalyst) and the formed coke exhibits heavier structures than those of TL (Fig. 8), being presumably located on the active sites within the micropores of the catalyst (Fig. 6).

5. Conclusions

A Pt-Pd catalyst supported on an acid activated carbon allows for achieving greater hydrodeoxygenation conversion values of raw bio-oil than those observed using an equilibrated FCC catalyst as support. These relatively high hydrodeoxygenation conversions lead to a liquid product predominantly consisting of water. However, the conditions of accelerated deactivation promote the production of high yields of gas and solid deposits compared to the liquid hydrocarbon one, whose properties make it interesting as a fuel. Conditions of favored coke formation also increase the possibilities for studying the whole spectrum of causes for catalyst deactivation, being able to identify two deactivating carbonaceous species with different location and nature on the porous texture of the support.

The instability of alkyl phenols and alkylmethoxy phenols (present in the bio-oil) leads to the deposition of thermal lignin on the external surface and the mesopores of the catalyst at 400 °C. This deactivating thermal lignin shows an aliphatic nature and high contents of oxygen. The deposition of thermal lignin causes a severe catalytic activity decay, which could lead in severe cases to a total reactor blockage by

these solids. At temperatures of about 450 °C, alkyl phenols and alkyl-methoxy phenols deoxygenate faster to form aromatic species leading to a drop in the formation rate of thermal lignin but an increase of aromatic coke deposition rate by subsequent condensations. This type of deactivating species has a more aromatic nature, less oxygen and its location is closer to the micropores of the catalyst. Based on the results of the characterization of product composition, used catalysts and carbonaceous species deposited on their surface, a scheme for the routes of coke formation is proposed. Two pathways are differentiated, whose contribution depends on the catalyst properties and the HDO temperature.

According to these two simultaneous deactivation pathways, avoiding fast deactivation by reaching a pseudo-steady conversion state turns out to be crucial for the implementation of the hydroprocessing of raw bio-oils in a continuous regime during a relatively long period of time. In this regard, a suppression of the alkyl phenols deactivation pathway is observed using a Pt-Pd supported catalyst above 450 °C, ensuring a unique and relatively slow deactivation pathway from alkyl aromatic species.

Acknowledgements

This work was carried out with the support of the Ministry of Economy and Competitiveness of the Spanish Government, some co-founded with ERDF funds (CTQ2015-67425-R, CTQ2015-68654-R and CTQ2016-79646-P) and the Basque Government (IT748-13). Dr. Idoia Hita is grateful for her postdoctoral grant awarded by the Department of Education, University and Research of the Basque Government (POS_2015_1_0035).

Appendix A. Supplementary data

Supplementary material related to this article can be found, in the online version, at doi:https://doi.org/10.1016/j.apcatb.2018.07.073.

References

[1] A.R.K. Gollakota, M. Reddy, M.D. Subramanyam, N. Kishore, A review on the upgradation techniques of pyrolysis oil, Renew. Sustain. Energy Rev. 58 (2016) 1543–1568.
[2] S. Oh, H.S. Choi, U.J. Kim, I.G. Choi, J.W. Choi, Storage performance of bio-oil after hydrodeoxygenative upgrading with noble metal catalysts, Fuel 182 (2016) 154–160.
[3] X. Zhang, W. Tang, Q. Zhang, Y. Li, L. Chen, Y. Xu, et al., Production of hydrocarbon fuels from heavy fraction of bio-oil through hydrodeoxygenative upgrading with Ru-based catalyst, Fuel 215 (2018) 825–834.
[4] P.L. Cruz, E. Montero, J. Dufour, Modelling of co-processing of HDO-oil with VGO in a FCC unit, Fuel 196 (2017) 362–370.
[5] H. Olcay, A.V. Subrahmanyam, R. Xing, J. Lajoie, J.A. Dumesic, G.W. Huber, Production of renewable petroleum refinery diesel and jet fuel feedstocks from hemicellulose sugar streams, Energy Environ. Sci. 6 (2013) 205–216.
[6] K.S. Arias, M.J. Climent, A. Corma, S. Iborra, Synthesis of high quality alkyl naphthenic kerosene by reacting an oil refinery with a biomass refinery stream, Energy Environ. Sci. 8 (2015) 317–331.
[7] E. Furimsky, Catalytic hydrodeoxygenation, Appl. Catal. A Gen. 199 (2000) 147–190.
[8] W. Zhang, Y. Zhang, L. Zhao, W. Wei, Catalytic activities of NiMo carbide supported on SiO2 for the hydrodeoxygenation of ethyl benzoate, acetone, and acetaldehyde, Energy Fuels 24 (2010) 2052–2059.
[9] M. Patel, A. Kumar, Production of renewable diesel through the hydroprocessing of lignocellulosic biomass-derived bio-oil: a review, Renew. Sustain. Energy Rev. 58 (2016) 1293–1307.
[10] H. Jahromi, F.A. Agblevor, Upgrading of pinyon-juniper catalytic pyrolysis oil via hydrodeoxygenation, Energy 141 (2017) 2186–2195.
[11] Y. Li, C. Zhang, Y. Liu, S. Tang, G. Chen, R. Zhang, et al., Coke formation on the surface of Ni/HZSM-5 and Ni-Cu/HZSM-5 catalysts during bio-oil hydro-deoxygenation, Fuel 189 (2017) 23–31.
[12] C. Guo, K.T.V. Rao, Z. Yuan, S. (Quan) He, S. Rohani, C. (Charles) Xu, Hydrodeoxygenation of fast pyrolysis oil with novel activated carbon-supported NiP and CoP catalysts, Chem. Eng. Sci. 178 (2018) 248–259.
[13] E.F. Iliopoulou, S.D. Stefanidis, K.G. Kalogiannis, A. Delimitis, A.A. Lappas, K.S. Triantafyllidis, Catalytic upgrading of biomass pyrolysis vapors using transition metal-modified ZSM-5 zeolite, Appl. Catal. B Environ. 127 (2012) 281–290.
[14] D.C. Elliott, T.R. Hart, G.G. Neuenschwander, L.J. Rotness, M.V. Olarte, A.H. Zacher, et al., Catalytic hydroprocessing of fast pyrolysis bio-oil from pine sawdust, Energy Fuels 26 (2012) 3891–3896.
[15] A. Sanna, T.P. Vispute, G.W. Huber, Hydrodeoxygenation of the aqueous fraction of bio-oil with Ru/C and Pt/C catalysts, Appl. Catal. B Environ. 165 (2015) 446–456.
[16] J. Wildschut, M. Iqbal, F.H. Mahfud, I.M. Cabrera, R.H. Venderbosch, H.J. Heeres, Insights in the hydrotreatment of fast pyrolysis oil using a ruthenium on carbon catalyst, Energy Environ. Sci. 3 (2010) 962–970.
[17] W. Nan, C.R. Krishna, T.J. Kim, L.J. Wang, D. Mahajan, Catalytic upgrading of switchgrass-derived pyrolysis oil using supported ruthenium and rhodium catalysts, Energy Fuels 28 (2014) 4588–4595.
[18] Y. Huang, L. Wei, X. Zhao, S. Cheng, J. Julson, Y. Cao, et al., Upgrading pine sawdust pyrolysis oil to green biofuels by HDO over zinc-assisted Pd/C catalyst, Energy Convers. Manag. 115 (2016) 8–16.
[19] S. Oh, H. Hwang, H.S. Choi, J.W. Choi, The effects of noble metal catalysts on the bio-oil quality during the hydrodeoxygenative upgrading process, Fuel 153 (2015) 535–543.
[20] K.A. Resende, C.A. Teles, G. Jacobs, B.H. Davis, D.C. Cronauer, A. Jeremy Kropf, et al., Hydrodeoxygenation of phenol over zirconia supported Pd bimetallic catalysts. The effect of second metal on catalyst performance, Appl. Catal. B Environ. 232 (2018) 213–231.
[21] Y. Luo, V.K. Guda, E.B. Hassan, P.H. Steele, B. Mitchell, F. Yu, Hydrodeoxygenation of oxidized distilled bio-oil for the production of gasoline fuel type, Energy Convers. Manag. 112 (2016) 319–327.
[22] M. Marafi, E. Furimsky, Hydroprocessing catalysts containing noble metals: deactivation, regeneration, metals reclamation, and environment and safety, Energy Fuels 31 (2017) 5711–5750.
[23] I. Hita, E. Rodríguez, M. Olazar, J. Bilbao, J.M. Arandes, P. Castaño, Prospects for obtaining high quality fuels from the hydrocracking of a hydrotreated scrap tires pyrolysis oil, Energy Fuels 29 (2015) 5458–5466.
[24] H. González, O.S. Castillo, J.L. Rico, A. Gutiérrez-Alejandre, J. Ramírez, Hydroconversion of 2-methylnaphthalene on pt/mordenite catalysts. Reaction study and mathematical modeling, Ind. Eng. Chem. Res. 52 (2013) 2510–2519.
[25] S. Gopal, P.G. Smirniotis, Deactivation behavior of bifunctional Pt/H-Zeolite catalysts during cyclopentane hydroconversion, J. Catal. 205 (2002) 231–243.
[26] P. Mäki-Arvela, G. Martin, I. Simakova, A. Tokarev, J. Wärnå, J. Hemming, et al., Kinetics, catalyst deactivation and modeling in the hydrogenation of β-sitosterol to β-sitostanol over microporous and mesoporous carbon supported Pd catalysts, Chem. Eng. J. 154 (2009) 45–51.
[27] H. Wang, Y. Wang, Characterization of deactivated bio-oil hydrotreating catalysts, Top. Catal. 59 (2016) 65–72.
[28] A.G. Gayubo, B. Valle, A.T. Aguayo, M. Olazar, J. Bilbao, Pyrolytic lignin removal for the valorization of biomass pyrolysis crude bio-oil by catalytic transformation, J. Chem. Technol. Biotechnol. 85 (2010) 132–144.
[29] A.H. Zacher, M.V. Olarte, D.M. Santosa, D.C. Elliott, S.B. Jones, A review and perspective of recent bio-oil hydrotreating research, Green Chem. 16 (2014) 491–515.
[30] D.C. Elliott, H. Wang, R. French, S. Deutch, K. Iisa, Hydrocarbon liquid production from biomass via hot-vapor-filtered fast pyrolysis and catalytic hydroprocessing of the bio-oil, Energy Fuels 28 (2014) 5909–5917.
[31] D.C. Elliott, H. Wang, M. Rover, L. Whitmer, R. Smith, R. Brown, Hydrocarbon liquid production via catalytic hydroprocessing of phenolic oils fractionated from fast pyrolysis of red oak and corn stover, ACS Sustain. Chem. Eng. 3 (2015) 892–902.
[32] H. Jahromi, F.A. Agblevor, Hydrodeoxygenation of pinyon-juniper catalytic pyrolysis oil using red mud-supported nickel catalysts, Appl. Catal. B Environ. 236 (2018) 1–12.
[33] O.D. Mante, F.A. Agblevor, S.T. Oyama, R. McClung, Catalytic pyrolysis with ZSM-5 based additive as co-catalyst to Y-zeolite in two reactor configurations, Fuel 117 (2014) 649–659.
[34] O.D. Mante, F.A. Agblevor, Catalytic pyrolysis for the production of refinery-ready biocrude oils from six different biomass sources, Green Chem. 16 (2014) 3364–3377.
[35] K. Wang, D.C. Dayton, J.E. Peters, O.D. Mante, Reactive catalytic fast pyrolysis of biomass to produce high-quality bio-crude, Green Chem. 19 (2017) 3243–3251.
[36] F.L.P. Resende, Recent advances on fast hydropyrolysis of biomass, Catal. Today 269 (2016) 148–155.
[37] T. Cordero-Lanzac, R. Palos, J.M. Arandes, P. Castaño, J. Rodríguez-Mirasol, T. Cordero, et al., Stability of an acid activated carbon based bifunctional catalyst for the raw bio-oil hydrodeoxygenation, Appl. Catal. B Environ. 203 (2017) 389–399.
[38] J. Bedia, R. Barrionuevo, J. Rodríguez-Mirasol, T. Cordero, Ethanol dehydration to ethylene on acid carbon catalysts, Appl. Catal. B Environ. 103 (2011) 302–310.
[39] C. Sepúlveda, K. Leiva, R. García, L.R. Radovic, I.T. Ghampson, W.J. Desisto, et al., Hydrodeoxygenation of 2-methoxyphenol over Mo2N catalysts supported on activated carbons, Catal. Today 172 (2011) 232–239.
[40] J.M. Rosas, J. Bedia, J. Rodríguez-Mirasol, T. Cordero, HEMP-derived activated carbon fibers by chemical activation with phosphoric acid, Fuel 88 (2009) 19–26.
[41] M.J. Valero-Romero, F.J. García-Mateos, J. Rodríguez-Mirasol, T. Cordero, Role of surface phosphorus complexes in the oxidation of porous carbons, Fuel Process. Technol. 157 (2017) 116–126.
[42] I. Hita, R. Palos, J.M. Arandes, J.M. Hill, P. Castaño, Petcoke-derived functionalized activated carbon as support in a bifunctional catalyst for tire oil hydroprocessing, Fuel Process. Technol. 144 (2016) 239–247.
[43] I.T. Ghampson, C. Sepúlveda, R. Garcia, L.R. Radovic, J.L.G. Fierro, W.J. Desisto, et al., Hydrodeoxygenation of guaiacol over carbon-supported molybdenum nitride catalysts: effects of nitriding methods and support properties, Appl. Catal. A Gen.

439–440 (2012) 111–124.
[44] H. Wan, R.V. Chaudhari, B. Subramaniam, Aqueous phase hydrogenation of acetic acid and its promotional effect on p-cresol hydrodeoxygenation, Energy Fuels 27 (2013) 487–493.
[45] C.R. Lee, J.S. Yoon, Y.-W. Suh, Ja.-W. Choi, J.-M. Ha, D.J. Suh, et al., Catalytic roles of metals and supports on hydrodeoxygenation of lignin monomer guaiacol, Catal. Commun. 17 (2012) 54–58.
[46] T. Cordero-Lanzac, I. Hita, A. Veloso, J.M. Arandes, J. Rodríguez-Mirasol, J. Bilbao, et al., Characterization and controlled combustion of carbonaceous deactivating species deposited on an activated carbon-based catalyst, Chem. Eng. J. 327 (2017) 454–464.
[47] M. Marafi, A. Stanislaus, Spent hydroprocessing catalyst management: a review. Part II. Advances in metal recovery and safe disposal methods, Resour. Conserv. Recycl. 53 (2008) 1–26.
[48] M. Breysse, P. Afanasiev, C. Geantet, M. Vrinat, Overview of support effects in hydrotreating catalysts, Catal. Today 86 (2003) 5–16.
[49] I. Hita, T. Cordero-Lanzac, A. Gallardo, J.M. Arandes, J. Rodríguez-Mirasol, J. Bilbao, et al., Phosphorus-containing activated carbon as acid support in a bi-functional Pt-Pd catalyst for tire oil hydrocracking, Catal. Commun. 78 (2016) 48–51.
[50] M.M. Sullivan, A. Bhan, Acetone hydrodeoxygenation over bifunctional metallic-acidic molybdenum carbide catalysts, ACS Catal. 6 (2016) 1145–1152.
[51] M.C. Edelman, M.K. Maholland, R.M. Baldwin, S.W. Cowley, Vapor-phase catalytic hydrodeoxygenation of benzofuran, J. Catal. 111 (1988) 243–253.
[52] F.E. Massoth, P. Politzer, M.C. Concha, J.S. Murray, J. Jakowski, J. Simons, Catalytic hydrodeoxygenation of methyl-substituted phenols: correlations of kinetic parameters with molecular properties, J. Phys. Chem. B 110 (2006) 14283–14291.
[53] O.I. Şenol, E.M. Ryymin, T.R. Viljava, A.O.I. Krause, Effect of hydrogen sulphide on the hydrodeoxygenation of aromatic and aliphatic oxygenates on sulphided catalysts, J. Mol. Catal. A Chem. 277 (2007) 107–112.
[54] E.M. Ryymin, M.L. Honkela, T.R. Viljava, A.O.I. Krause, Competitive reactions and mechanisms in the simultaneous HDO of phenol and methyl heptanoate over sulphided NiMo/γ-Al2O3, Appl. Catal. A Gen. 389 (2010) 114–121.
[55] M. Saidi, F. Samimi, D. Karimipourfard, T. Nimmanwudipong, B.C. Gates, M.R. Rahimpour, Upgrading of lignin-derived bio-oils by catalytic hydrodeoxygenation, Energy Environ. Sci. 7 (2014) 103–129.
[56] R.C. Runnebaum, T. Nimmanwudipong, D.E. Block, B.C. Gates, Catalytic conversion of compounds representative of lignin-derived bio-oils: a reaction network for guaiacol, anisole, 4-methylanisole, and cyclohexanone conversion catalysed by Pt/γ-Al_2O_3, Catal. Sci. Technol. 2 (2012) 113–118.
[57] G.S. Foo, A.K. Rogers, M.M. Yung, C. Sievers, Steric effect and evolution of surface species in the hydrodeoxygenation of bio-oil model compounds over Pt/HBEA, ACS Catal. (2016) 1292–1307.
[58] P.M. Mortensen, J.D. Grunwaldt, P.A. Jensen, K.G. Knudsen, A.D. Jensen, A review of catalytic upgrading of bio-oil to engine fuels, Appl. Catal. A Gen. 407 (2011) 1–19.
[59] P.A. Alaba, Y.M. Sani, I.Y. Mohammed, W.M.A. Wan Daud, Insight into catalyst deactivation mechanism and suppression techniques in thermocatalytic deoxygenation of bio-oil over zeolites, Int. Rev. Chem. Eng. 32 (2016) 71–91.
[60] S. Cheng, L. Wei, X. Zhao, J. Julson, Application, deactivation, and regeneration of heterogeneous catalysts in bio-oil upgrading, Catalysts 6 (2016) 195–219.
[61] R. Palos, A. Gutiérrez, J.M. Arandes, J. Bilbao, Catalyst used in fluid catalytic cracking (FCC) unit as a support of NiMoP catalyst for light cycle oil hydroprocessing, Fuel 216 (2018) 142–152.
[62] A.R. Fernandez-Akarregi, J. Makibar, G. Lopez, M. Amutio, M. Olazar, Design and operation of a conical spouted bed reactor pilot plant (25 kg/h) for biomass fast pyrolysis, Fuel Process. Technol. 112 (2013) 48–56.
[63] A.G. Marshall, R.P. Rodgers, Petroleomics: the next grand challenge for chemical analysis, Acc. Chem. Res. 37 (2004) 53–59.
[64] E.A. Smith, Y.J. Lee, Petroleomic analysis of bio-oils from the fast pyrolysis of biomass: laser desorption ionization-linear ion trap-orbitrap mass spectrometry approach, Energy Fuels 24 (2010) 5190–5198.
[65] M. Staš, J. Chudoba, M. Auersvald, D. Kubička, S. Conrad, T. Schulzke, et al., Application of orbitrap mass spectrometry for analysis of model bio-oil compounds and fast pyrolysis bio-oils from different biomass sources, J. Anal. Appl. Pyrolysis 124 (2017) 230–238.
[66] E. Furimsky, Deactivation of molybdate catalyst during hydrodeoxygenation of tetrahydrofuran, Ind. Eng. Chem. Prod. Res. Dev. 22 (1983) 34–38.
[67] H.S. Cerqueira, C. Sievers, G. Joly, P. Magnoux, J.A. Lercher, Multitechnique characterization of coke produced during commercial resid FCC operation, Ind. Eng. Chem. Res. 44 (2005) 2069–2077.
[68] A. Ochoa, B. Aramburu, M. Ibáñez, B. Valle, J. Bilbao, A.G. Gayubo, et al., Compositional insights and valorization pathways for carbonaceous material deposited during bio-oil thermal treatment, ChemSusChem 7 (2014) 2597–2608.
[69] P.M. De Souza, R.C. Rabelo-neto, L.E.P. Borges, G. Jacobs, B.H. Davis, D.E. Resasco, et al., Hydrodeoxygenation of phenol over Pd catalysts. Effect of support on reaction mechanism and catalyst deactivation, ACS Catal. (2017) 2–3.
[70] R.Y. Nsimba, C.A. Mullen, N.M. West, A.A. Boateng, Structure-property characteristics of pyrolytic lignins derived from fast pyrolysis of a lignin rich biomass extract, ACS Sustain. Chem. Eng. 1 (2013) 260–267.
[71] A.E. Pütün, E. Apaydin, E. Pütün, Bio-oil production from pyrolysis and steam pyrolysis of soybean-cake: product yields and composition, Energy 27 (2002) 703–713.
[72] P. Das, T. Sreelatha, A. Ganesh, Bio oil from pyrolysis of cashew nut shell-characterisation and related properties, Biomass Bioenergy 27 (2004) 265–275.
[73] S. Zou, Y. Wu, M. Yang, C. Li, J. Tong, Bio-oil production from sub- and supercritical water liquefaction of microalgae Dunaliella tertiolecta and related properties, Energy Environ. Sci. 3 (2010) 1073–1078.
[74] C. Lievens, D. Mourant, M. He, R. Gunawan, X. Li, C.Z. Li, An FT-IR spectroscopic study of carbonyl functionalities in bio-oils, Fuel 90 (2011) 3417–3423.
[75] B. Valle, P. Castaño, M. Olazar, J. Bilbao, A.G. Gayubo, Deactivating species in the transformation of crude bio-oil with methanol into hydrocarbons on a HZSM-5 catalyst, J. Catal. 285 (2012) 304–314.
[76] S. Echeandia, P.L. Arias, V.L. Barrio, B. Pawelec, J.L.G. Fierro, Synergy effect in the HDO of phenol over Ni-W catalysts supported on active carbon: effect of tungsten precursors, Appl. Catal. B Environ. 101 (2010) 1–12.